Supplementary Information:

Conducting oxide surface engineering enables growth of low-defect carbon nitride film for unbiased photoelectrochemical water splitting

Suqin Wu,[#,a] Wenjie Deng,[#,a] Chen Lai,[#,a] Fengmei Zhi,[a] Shuai Xiong,[a] Shubin Xiong,[a] Mao He,[a] Menny Shalom,[b] and Guiming Peng[a,*]

[a]*College of Chemistry and Materials, National Engineering Research Center for Carbonhydrate Synthesis, Key Lab of Fluorine and Silicon for Energy Materials and Chemistry of Ministry of Education, Laboratory of Green Catalysis of Jiangxi Education Institutes, Jiangxi Normal University, Nanchang 330022, China*
E-mail: guiming@jxnu.edu.cn
[b]Department of Chemistry and Ilse Katz Institute for Nanoscale Science and Technology, Ben-Gurion University of the Negev, Beer-Sheva 8410501, Israel.
[#]These authors contributed equally to this work.

Experimental Section

Materials

Chemicals were used as received with no further purification. Melamine, dicyandiamide, urea, thiourea were purchased from Sigma-Aldrich Ltd. Zn powder was purchased from Infinity Scientific Ltd. Fluorine-doped tin oxide (FTO) glass (12-14 Ω cm^{-2}) was purchased from GULUO Glass company. Before using, the FTO glass slides were thoroughly washed with aqueous detergent solution, acetone, and ethanol sequentially. Deionized water (18.2 MΩ·cm at 25 ˚C) was used throughout the whole research.

Fabrication of etched FTO

To modulate the surface state of FTO, the pristine FTO was etched by hydrochloric acid mixed with zinc powder. Typically, after spreading zinc powder on FTO surface, 0.5 M HCl was drop-cast on it and held for 10 seconds. Then the surface was quickly washed with DI water to remove the residual reactants. Afterwards, the etched FTO slides were ultrasonically cleaned in acetone and ethanol for 30 min, respectively, and dried with nitrogen gas before use.

Synthesis of E-CN film

The E-CN film was synthesized by chemical vapor assisted deposition method. Generally, melamine (2 g) was put at the bottom of a test tube while the etched FTO glass was positioned in the same test tube but without direct contact with the precursor. After sealed with aluminum foil, the system was heated to 550 °C at a ramping rate of 5 °C min^{-1}, and then maintained at 550 °C for 4 h in N_2 atmosphere. After cooling down, the as-prepared E-CN film on etched FTO was obtained.

Synthesis of NiCo-LDH/E-CN

The aqueous mixture of 0.15 M $Co(NO_3)_2$ and 0.15 M $Ni(NO_3)_2$ was used as electrolyte. NiCo-LDH was then electrodeposited onto the E-CN film at -1.0 V vs RHE with total charge of 0.1 C. After that, the obtained NiCo-LDH/E-CN was washed with DI water before use.

Materials characterization

The morphology of the materials was examined by scanning electron microscopy (SEM, Tescan Clara). The X-ray diffractometer (XRD) patterns were recorded on a Bruker D8 Advance diffractometer (Cu Kα X-ray radiation, $\lambda = 1.54$ Å) at a rate of 10°min^{-1} at the voltage of 40 kV and current of 40 mA. Fourier transform infrared spectra (FTIR) was obtained on a Spectrum One spectrometer. UV-vis spectra were obtained using a Shimadzu UV-2600i UV-Vis-NIR spectrophotometer. Fluorescence measurements were collected using an Edinburgh instruments FLS920P Fluorimeter. Gas chromatography (GC) data was collected using a FULI GC9790II.

Photoelectrochemical measurements

All electrochemical measurements were conducted using a three-electrode system on a potentiostat (CHI 760E). A Pt foil electrode and an Ag/AgCl (saturated KCl) electrode were used as the counter and reference electrode, respectively. All of the potentials were converted to reverse hydrogen electrode (RHE) values using $V_{RHE} = V_{Ag/AgCl} + 0.059pH + 0.197$. Mott-Schottky measurements were performed in 0.1 M Na_2SO_4 aqueous solution using the same potentiostat. Photocurrents were measured at 1.23 V vs RHE under the illumination of a solar simulator (PerfectLight 300 W Xe lamp) at the power density of 100 mW cm^{-2}, which was calibrated using a power meter (Model FZ-A, PerfectLight). Incident photon-to-current conversion efficiency (IPCE) values were obtained following the below equation:

$$IPCE\ (\%) = \left[(J_{light} \times 1240)/(\lambda \cdot P_{\lambda})\right] \cdot 100\%$$

where λ is the wavelength of the incident monochromic light, P_{λ} is the power density of the incident light (mW cm^{-2}), J_{light} is the photocurrent density (mA cm^{-2}). The monochromic incident lights with different wavelengths of 400 nm, 420 nm, 450 nm, 475 nm, 500 nm are generated by coupling the solar simulator with the corresponding photo filters. The applied bias photon-to-current efficiencies (ABPE) were calculated using the following equation:

$$ABPE\ (\%) = \left[(1.23 - V_{app}) \times J_{light}/P_{light}\right] \cdot 100\%$$

where V_{app} is the applied potential, J_{light} is the photocurrent density (mA cm^{-2}), and P_{light} is the power density of the incident light (100 mW cm^{-2}). Hole extraction efficiency was calculated using the equation:

$$\eta\ (\%) = \left(J_{KOH}/J_{TEOA}\right) \cdot 100\%$$

on assumption that the photocurrent obtained in presence of hole scavenger (10% TEOA in electrolyte) representing full hole extraction. J_{KOH} is the photocurrent obtained in 0.1 M KOH aqueous solution, while J_{TEOA} is the photocurrent obtained in 10% TEOA contained 0.1 M KOH aqueous solution.

Density Functional Theory (DFT) Calculation

All the DFT calculations were conducted based on the Vienna Ab-inito Simulation Package (VASP).[1, 2] The exchange-correlation effects were described by the Perdew-Burke-Ernzerhof (PBE) functional within the generalized gradient approximation (GGA) method.[3, 4] The core-valence interactions were accounted by the projected augmented wave (PAW) method.[5] The energy cutoff for plane wave expansions was set to 400 eV. The structural optimization was completed for energy and force convergence set at 1.0×10^{-6} eV and 0.05 eV

Å^{-1}, respectively. The bulk of SnO_2 was constructed with lattice parameters of a = b = 4.476 Å, c = 3.207 Å, α = β = γ = 90°. The (110), (200), and (211) surfaces were cleaved and the model of C_3N_4 was constructed form previous literature.[6] The Brillouin zone was sampled with a 1 × 1 × 1 grid centered at the gamma (Γ) point. The adsorption energy (E_{ads}) of C_3N_4 on the SnO_2 (110), SnO_2 (200), and SnO_2 (211) surfaces were calculated by the following formula:

$$E_{ads} = E_{total} - E_s - E_{C_3N_4}$$

where E_{total} is the total energy of the surface and C_3N_4, the E_s is the energy of the surface, and the $E_{C_3N_4}$ is the energy of C_3N_4.

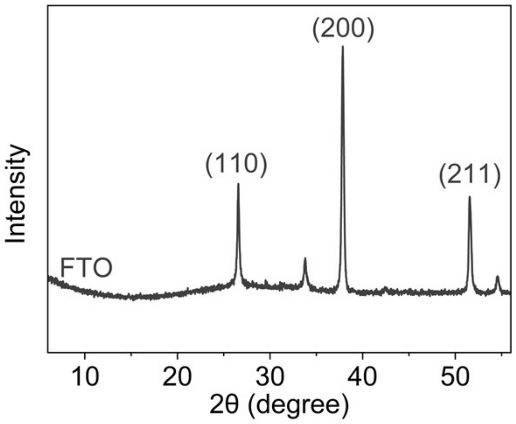

Figure S1. XRD pattern of pristine FTO.

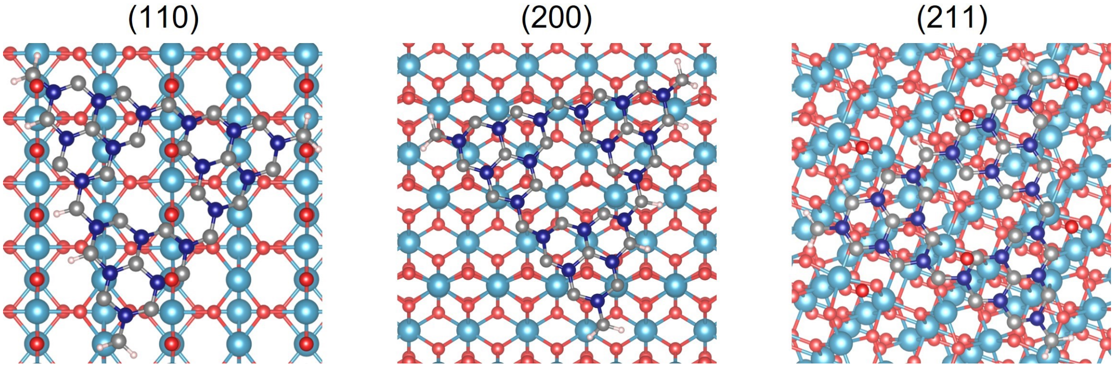

Figure S2. Top view adsorption configurations of C_3N_4 on SnO_2 (110), (200), and (211) surfaces.

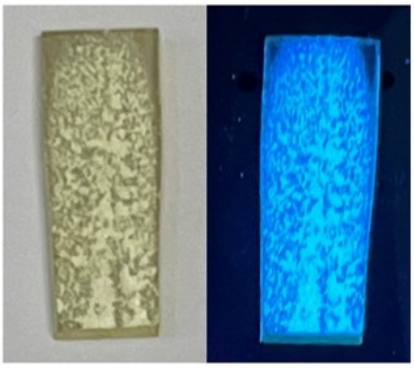

Figure S3. Photographs of CN film grown on pristine FTO with and without illumination at 365 nm.

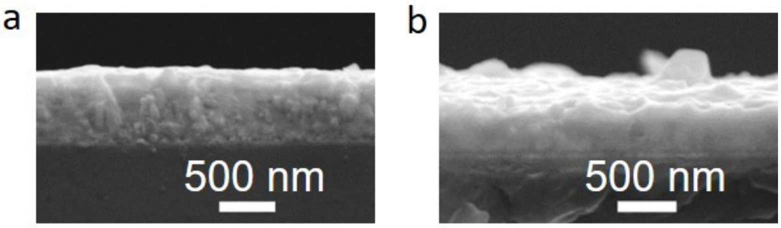

Figure S4. Cross-section SEM images of (a) pristine FTO and (b) etched FTO.

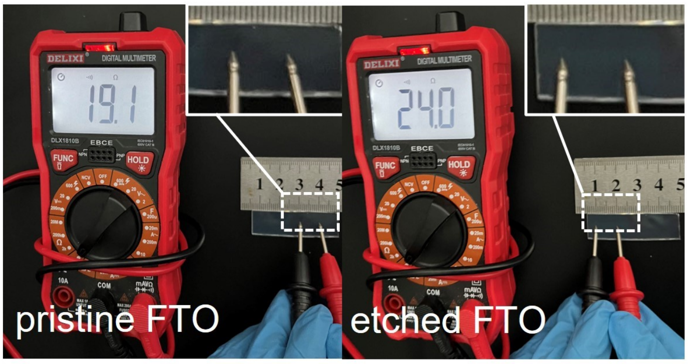

Figure S5. Surface resistance of pristine FTO and etched FTO.

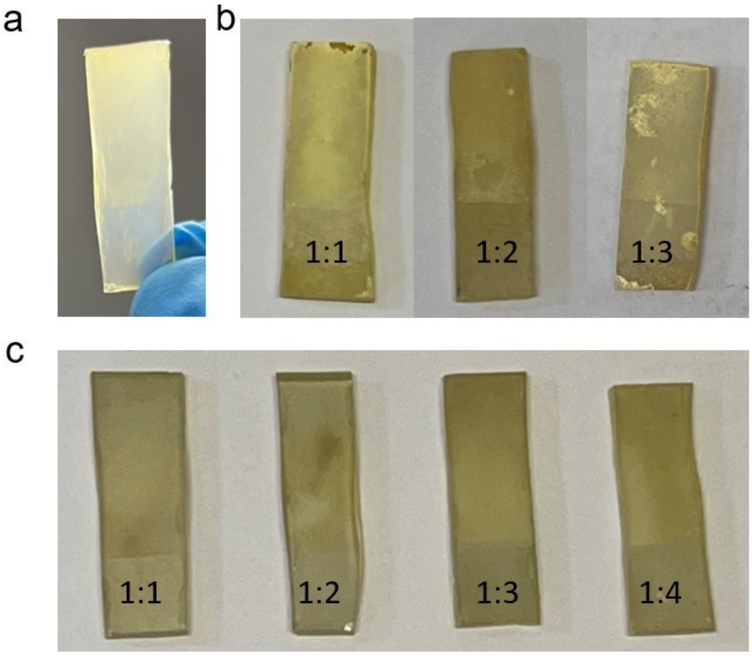

Figure S6. Photographs of CN films grown on etched FTO by using different precursors. (a) CN film synthesized by using urea as precursor. (b) CN films synthesized by using mixtures of melamine and thiourea at different mass ratios (1:1, 1:2, 1:3) as precursors. (c) CN films synthesized by using mixtures of melamine and urea at different mass ratios (1:1, 1:2, 1:3, 1:4) as precursors. Obviously, it can be observed that the uniform CN films were successfully synthesized on the etched area on FTO, different from the pristine area.

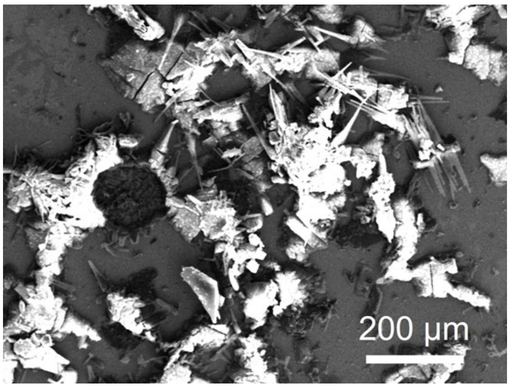

Figure S7. Top-view SEM image of CN structures grown on pristine FTO.

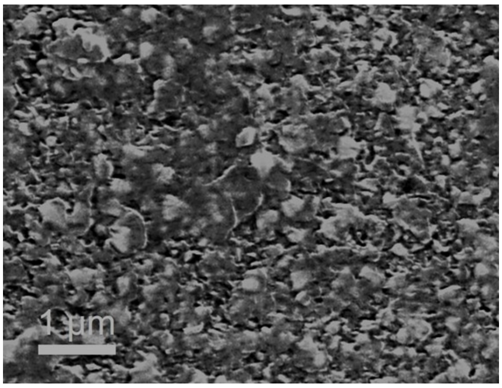

Figure S8. SEM image of E-CN residue on etched FTO after removal of most E-CN.

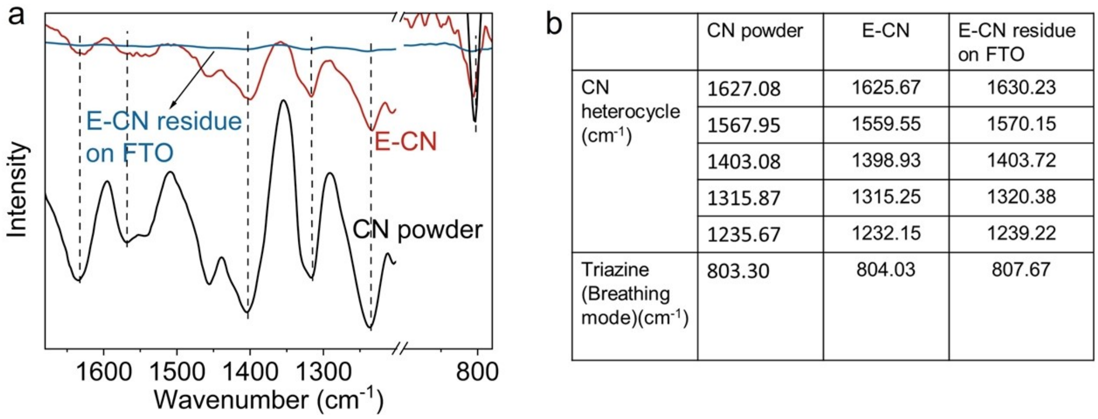

	CN powder	E-CN	E-CN residue on FTO
CN heterocycle (cm^{-1})	1627.08	1625.67	1630.23
	1567.95	1559.55	1570.15
	1403.08	1398.93	1403.72
	1315.87	1315.25	1320.38
	1235.67	1232.15	1239.22
Triazine (Breathing mode)(cm^{-1})	803.30	804.03	807.67

Figure S9. (a) FTIR spectra of CN powder, E-CN and the E-CN residue on etched FTO after removal of most E-CN. (b) Attributions of the FTIR characteristic peaks for CN powder, E-CN and the E-CN residue on etched FTO after removal of most E-CN.

The peak at 804 cm^{-1} is indexed to the breathing mode of the heptazine unit, while the characteristic bands at 3000-3400 cm^{-1} are attributed to -NH$_x$ groups. The C-N heterocycles peaks are found at 1200-1700 cm^{-1}.[7] These FTIR characteristic peaks confirm the formation of CN.

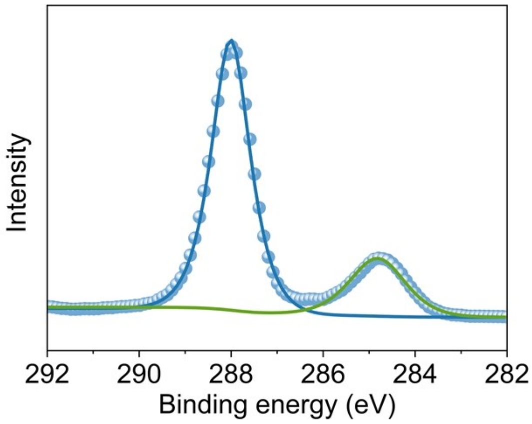

Figure S10. C1s XPS spectra of E-CN.

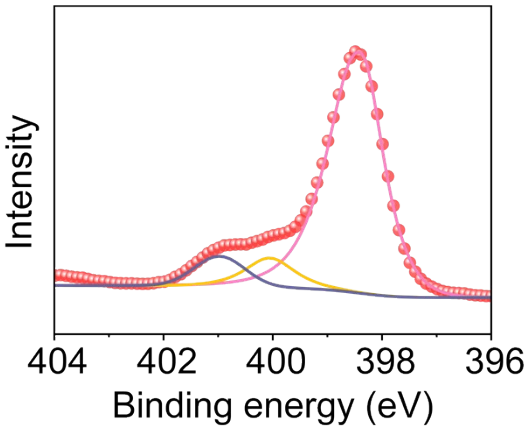

Figure S11. N1s XPS spectra of E-CN.

C1s XPS spectra shows two peaks at 284.8 and 288.0 eV, corresponding to C-C and C=N bonds, respectively (Figure S10).[8] The three deconvoluted peaks at 398.4, 400, and 400.9 eV in N 1s XPS spectra belong to C=N-C, N-C$_3$, and C-NH$_x$, respectively (Figure S11).[9]

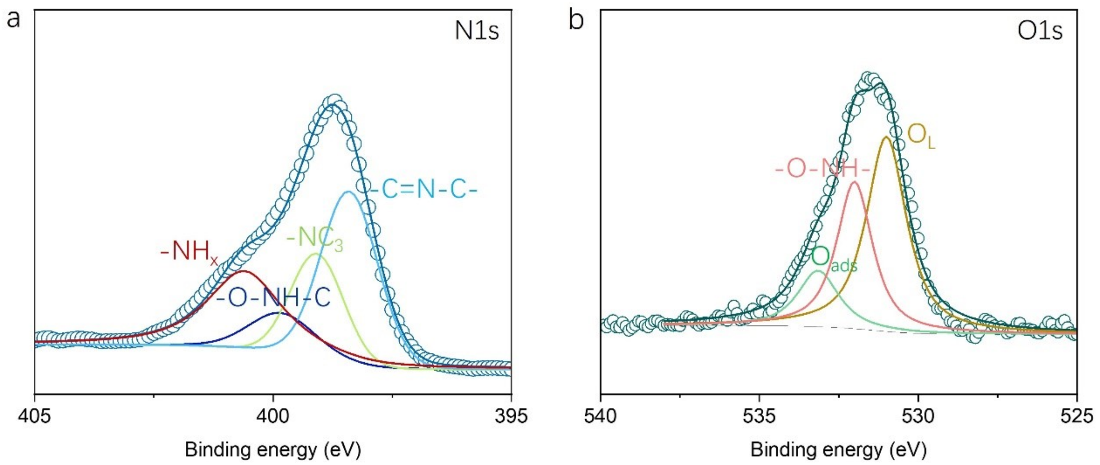

Figure S12. XPS of CN residue on FTO. (a) N1s XPS spectra, (b) O1s XPS spectra.

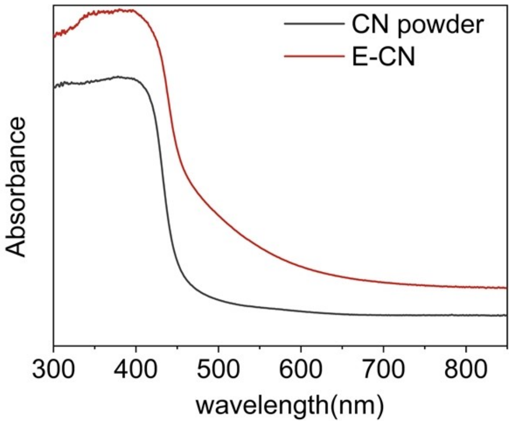

Figure S13. UV-vis plots of E-CN and CN powder synthesized by calcination of melamine.

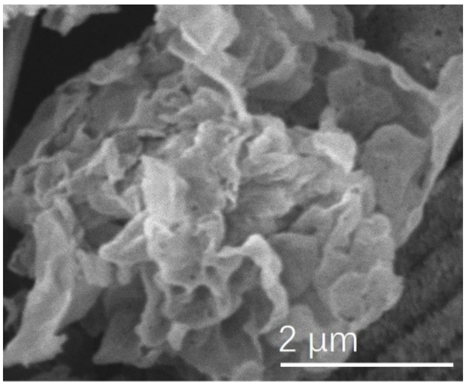

Figure S14. SEM image of CN powder.

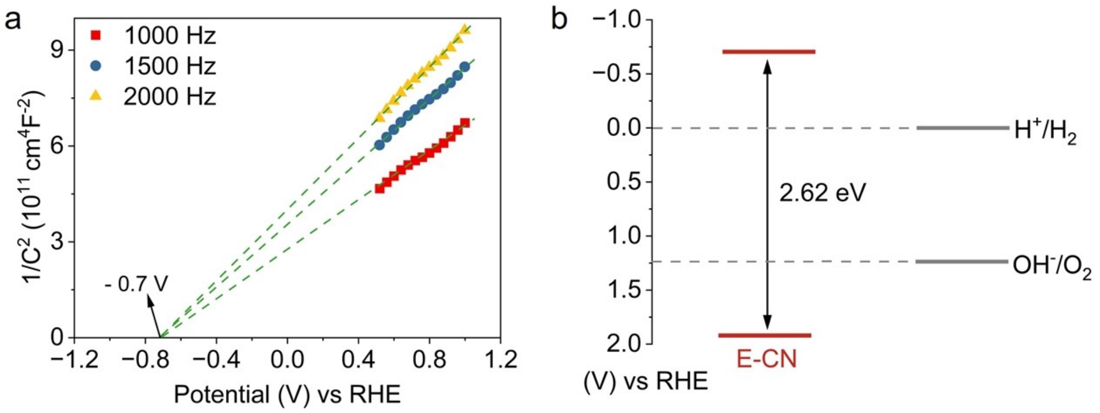

Figure S15. (a) Mott-Schottky plot of the E-CN. (b) Bandgap diagram of the E-CN with respect to that of water redox potentials.

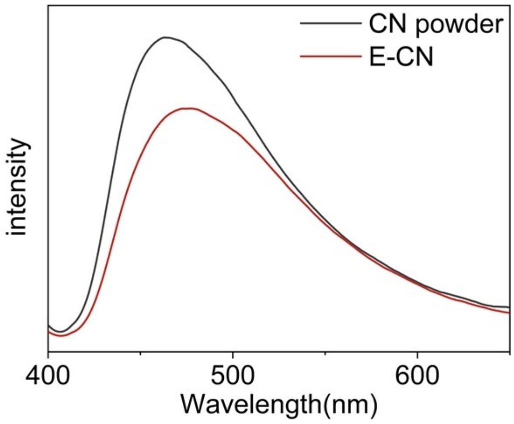

Figure S16. Fluorescence spectra of E-CN and CN powder.

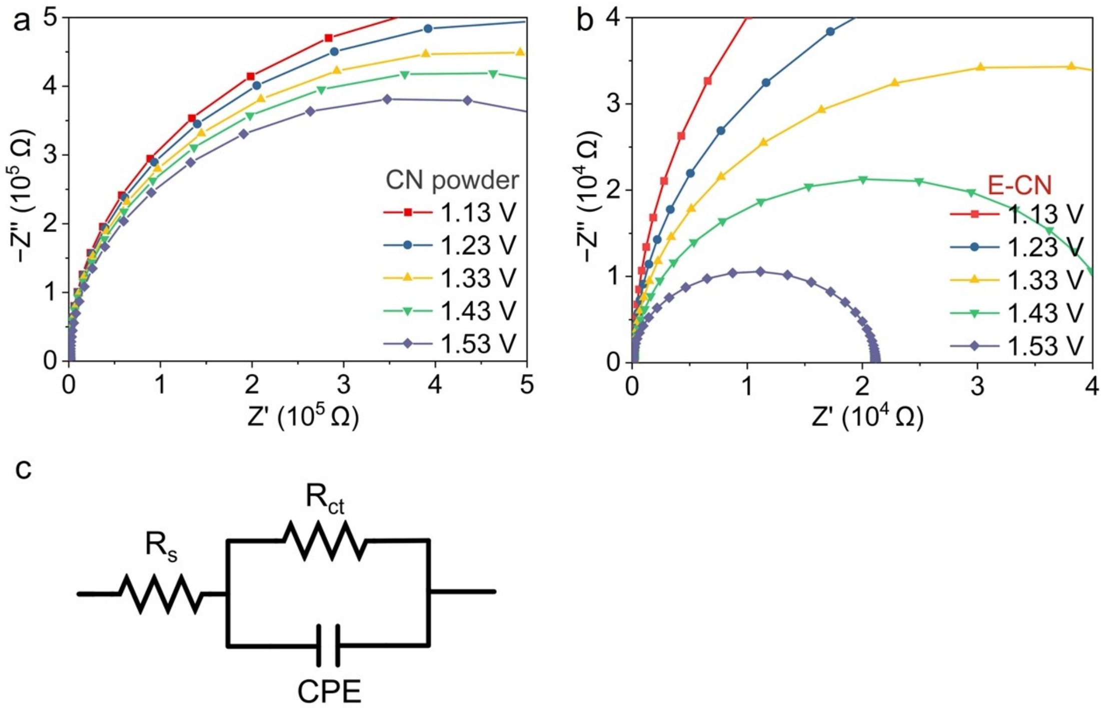

Figure S17. Nyquist plots of (a) CN powder, and (b) E-CN at different potentials (vs. RHE) in 0.1 M KOH aqueous solution. (c) The equivalent circuit for the fitting of Nyquist plots.

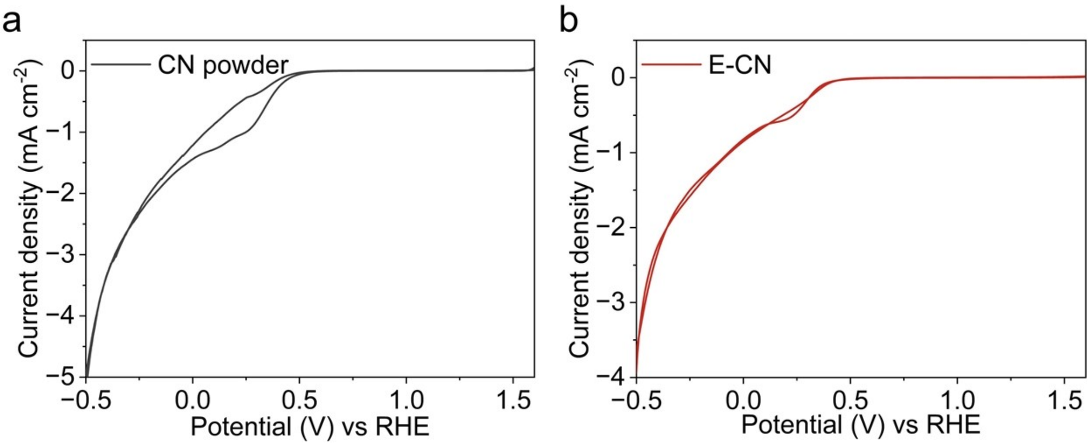

Figure S18. Cyclic voltammetry curve of (a) CN powder and (b) E-CN in 0.1 M KOH aqueous solution. The scan rate is 2 mV/s.

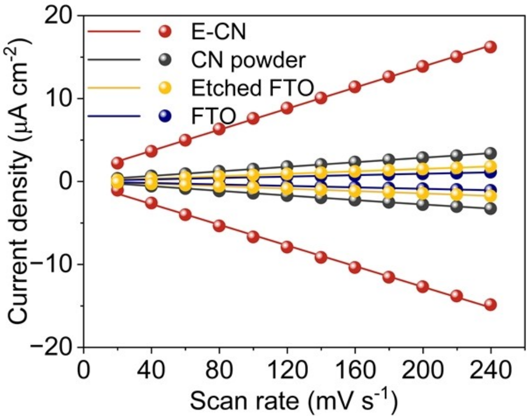

Figure S19. Cathodic and anodic charging currents of FTO, etched FTO, CN powder, E-CN, and NiCo-LDH/E-CN electrodes measured at 1.1 V vs RHE as a function of scan rates.

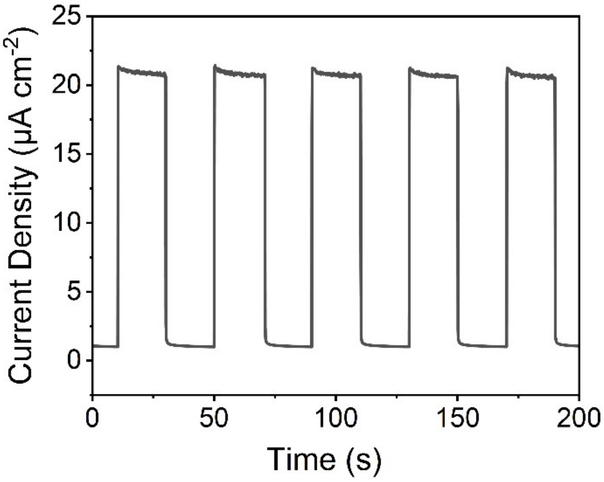

Figure S20. Photocurrent of CN islands on pristine FTO.

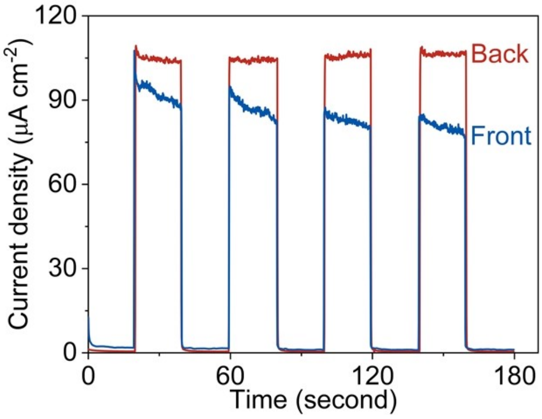

Figure S21. Photocurrent densities when illuminated from front- and back-side of E-CN electrode at 1.23 V vs RHE in 0.1 M KOH.

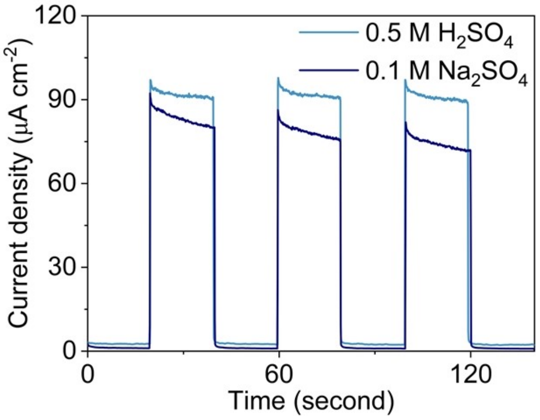

Figure S22. Photocurrent of E-CN at 1.23 V vs RHE in 0.1 M Na_2SO_4 and 0.5 M H_2SO_4 aqueous solutions upon 1 sun illumination.

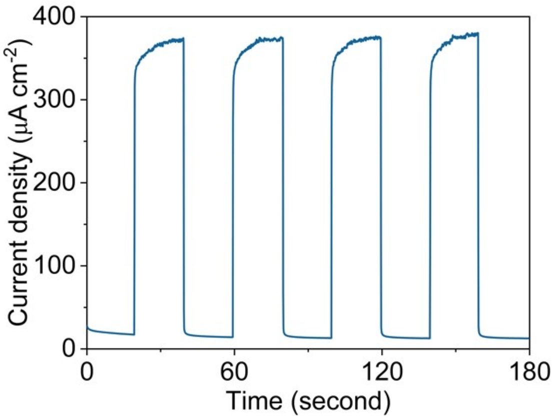

Figure S23. Photocurrent of the E-CN at 1.23 V vs RHE in 0.1 M KOH aqueous solution containing 10% (v/v) TEOA upon 1 sun illumination.

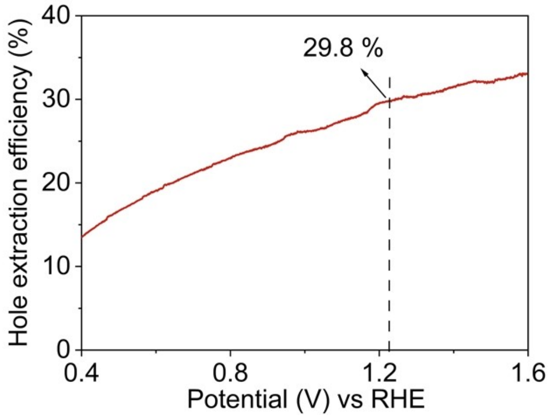

Figure S24. The hole extration efficiency (defined as the ratio between the photocurrent in 0.1 M KOH and that in 0.1 M KOH containing the hole scavenger) plot of E-CN.

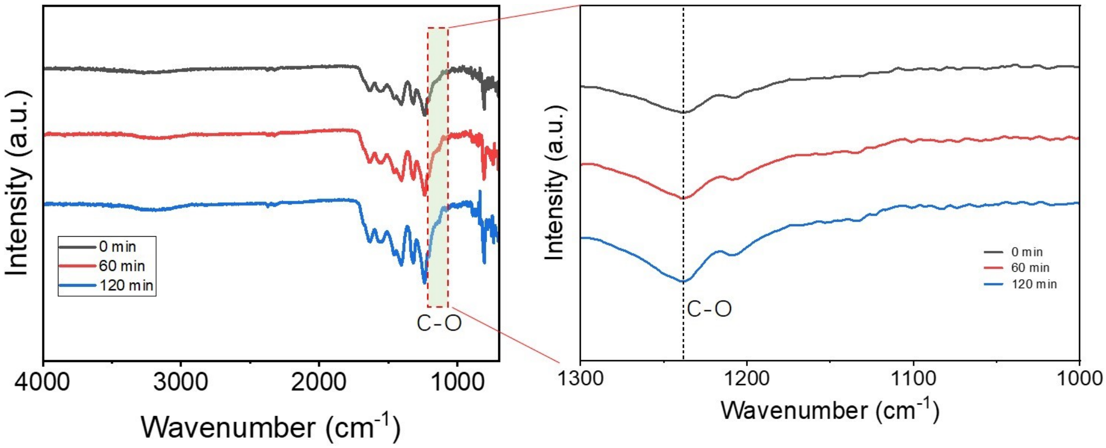

Figure S25. FTIR characterization of E-CN after PEC test.

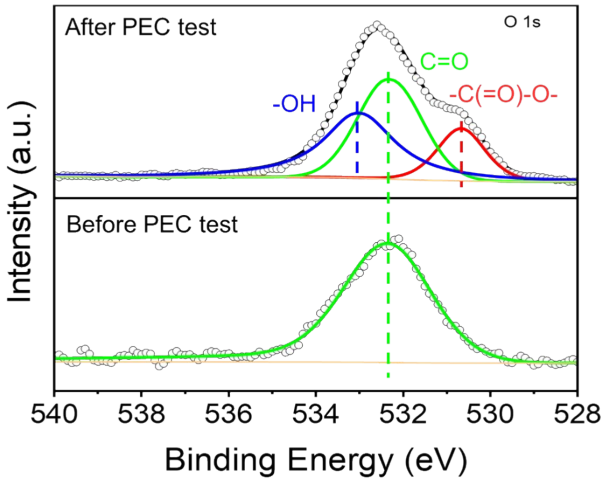

Figure S26. O1s XPS spectra of E-CN before and after PEC test.

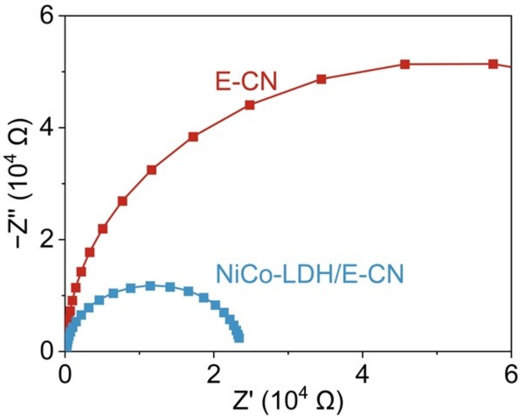

Figure S27. Nyquist plots of E-CN and NiCo-LDH/E-CN.

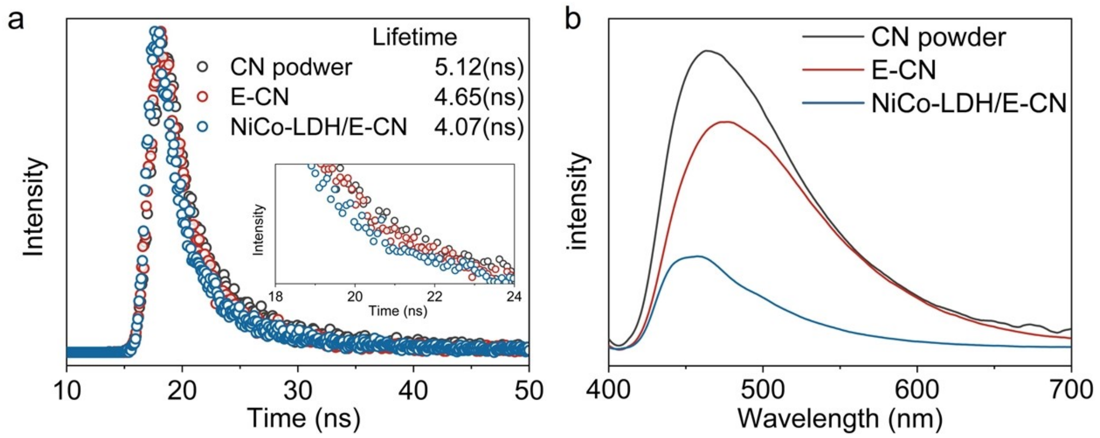

Figure S28. (a) PL decay curves and (b）Fluorescence spectra of NiCo-LDH/E-CN, E-CN and CN powder.

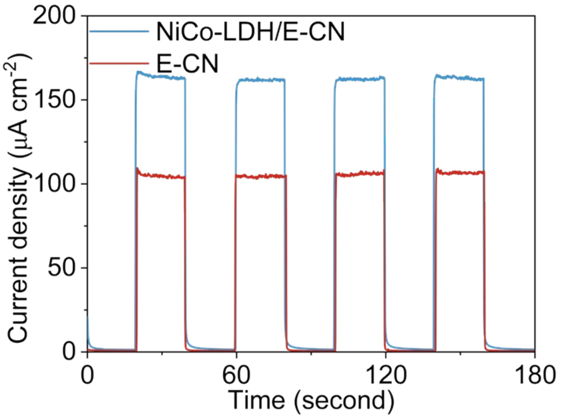

Figure S29. Photocurrent of E-CN and NiCo-LDH/E-CN at 1.23 V vs RHE in 0.1 M KOH.

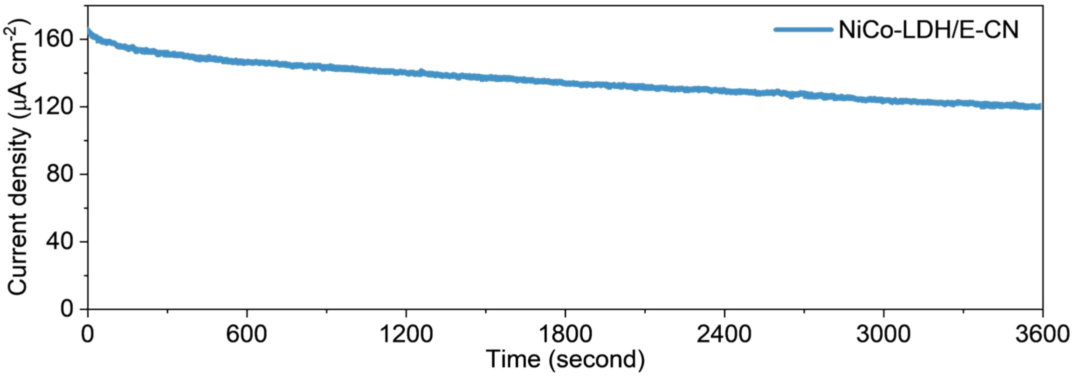

Figure S30. Photocurrent stability of the NiCo-LDH/E-CN electrode upon continuous 1-sun illumination in 0.1 M KOH aqueous solution.

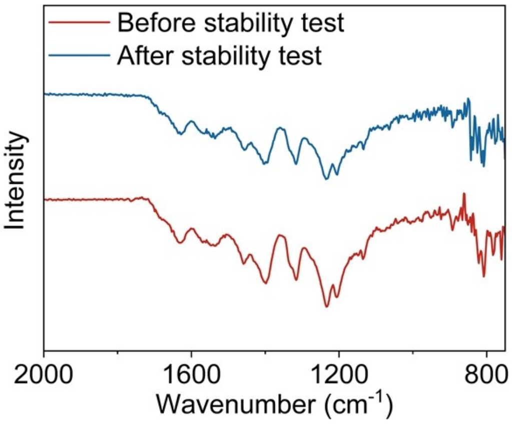

Figure S31. FTIR spectra of NiCo-LDH/E-CN before and after photocurrent stability test.

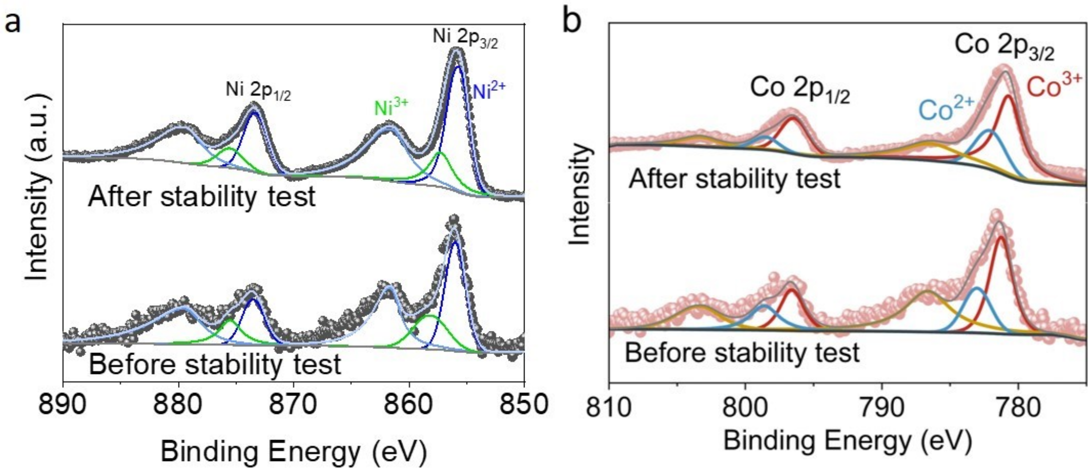

Figure S32. High-resolution (a) Ni 2p and (b) Co 2p XPS spectra of NiCo-LDH/E-CN before and after PEC water splitting.

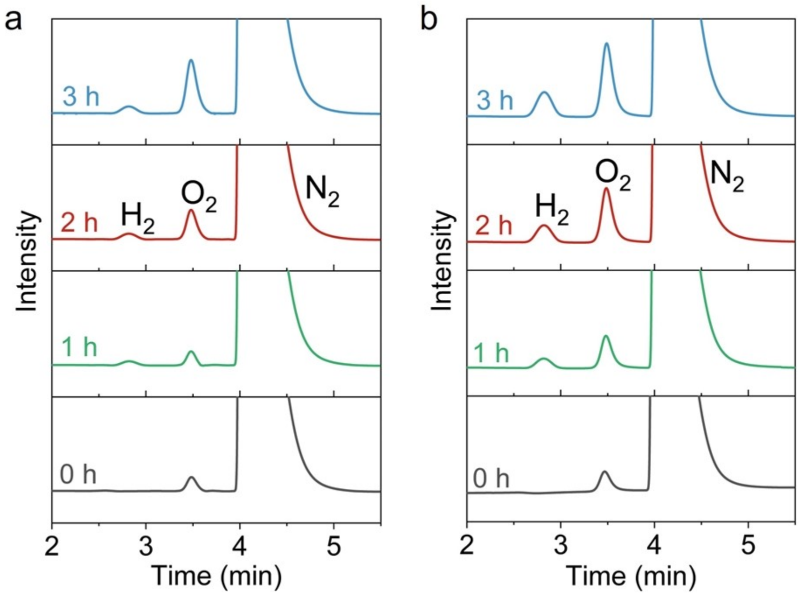

Figure S33. Gas chromatograms after different photoelectrochemical measurement durations (0, 1, 2, and 3 h) when using (a) E-CN in 0.1 M KOH solution and (b) E-CN in 0.1 M KOH containing 10% (v/v) TEOA. The electrodes are biased at 1.23 V vs RHE under 1-sun illumination.

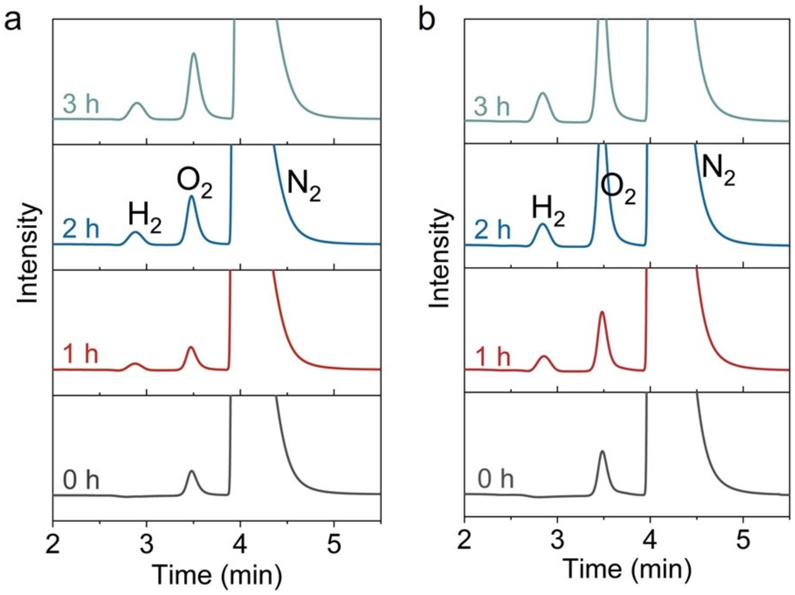

Figure S34. Gas chromatograms after different photoelectrochemical measurement durations (0, 1, 2, and 3 h) when using (a) NiCo-LDH/E-CN in 0.1 M KOH solution and (b) NiCo-LDH/E-CN in 0.1 M KOH containing 10% (v/v) TEOA. The electrodes are biased at 1.23 V vs RHE under 1-sun illumination.

Table S1. Photovoltages of representative CN bare photoanodes. Photoanodes of CN composited with other materials or different CN materials are not included here.

Photoanode	Photovoltage (V)	Electrolyte	Light source	Ref.
E-CN film	**0.64**	**0.1 M KOH**	**100 mW cm^{-2}**	**This work**
CN film	0.49	0.5 M H_2SO_4	100 mW cm^{-2}, AM 1.5	*Angew. Chem. Int. Ed.* **2022**, *61*, e202204407.
Crystalline CN film	0.61	0.1 M KOH	100 mW cm^{-2}, AM 1.5	*Angew. Chem. Int. Ed.* **2018**, *57*, 15807-15811.
CN/rGO$_{0.5}$ film	0.58	0.1 M KOH	100 mW cm^{-2}, AM 1.5	*J. Mater. Chem. A* **2019**, *7*, 11718-11723.
CN film	0.18	0.5 M Na_2SO_4	100 mW cm^{-2}	*J. Phys. Chem. C* **2019**, *123*, 26106-26115.
CN film	0.13	0.1 M Na_2SO_4	100 mW cm^{-2}, AM 1.5	*Appl. Surf. Sci.* **2016**, *389*, 1076-1083.
CN/TiO_2	0.2	0.5 M Na_2SO_4	90 mW cm^{-2}	*Dalton Trans.* **2016**, *45*, 12702-12709.
CN	0.46	1 M KOH	100 mW cm^{-2}, AM 1.5	*Chem. Mater.* **2023**, *8*, e202203688.
CNQD@ZnO	0.24	0.1 M KOH	100 mW cm^{-2}, AM 1.5	*Carbon* **2021**, *173*, 339-349.
CN film	0.07	0.1 M KOH	100 mW cm^{-2}, AM 1.5	*Chem. Mater.* **2020**, *32*, 5845-5853.
TiO_2@CN	0.53	0.5 M Na_2SO_4	100 mW cm^{-2}, AM 1.5	*Nanoscale* **2018**, *10*, 3342-3349.

Table S2. PEC performances of representative CN based photoanodes

Photoanode	Photocurrent (mA/cm^2)	Electrolyte	Potential (V vs. RHE)	Light source	Ref.
E-CN	**0.108**	**0.1 M KOH**	**1.23**	**100 mW cm^{-2}, AM1.5G**	**This work**
NiCo-LDH/E-CN	**0.162**	**0.1 M KOH**	**1.23**	**100 mW cm^{-2}, AM1.5G**	**This work**
CN/rGO	0.072	0.1 M KOH	1.23	100 mW cm^{-2}, AM1.5	*Adv. Energy Mater.* **2018**, *8*, 1800566.
M-LCN	0.073	0.1 M NaOH	1.23	100 mW cm^{-2}, AM1.5G	*Carbon Energy* **2022**, *4*, 1228–1241
PCN	0.1	1 M KOH	1.23	100 mW cm^{-2}, AM 1.5G	*ACS Catal.* **2018**, *8*, 8774–8780.
s-BCN	0.103	0.1 M Na_2SO_4	1.23	100 mW cm^{-2}, AM 1.5G	*Angew. Chem. Int. Ed.* **2017**, *56*, 8221 –8225.
SOCN-75	0.119	0.2 M Na_2SO_4	1.23	100 mW cm^{-2}, AM1.5G	*J. Mater. Chem. A* **2020**, *8*, 24005-24012.
3MelM$_{680/10}$	0.12	0.1 M KOH	1.23	100 mW cm^{-2}, AM1.5	*Small Struct.* **2024**, *5*, 2400123.
CN/rGO$_{0.5}$	0.124	0.1 M KOH	1.23	100 mW cm^{-2}, AM1.5G	*J. Mater. Chem. A* **2019**, *7*, 11718-11723.
CN-MeM/M$_{0.20}$	0.133	0.1 M KOH	1.23	100 mW cm^{-2}, AM1.5G	*Chem. Mater.* **2020**, *32*, 5845-5853.

$\mathrm{CN_{M+mIm}}$	0.16	0.1 M KOH	1.23	100 mW cm^{-2}, AM1.5G	*Mater. Horizons* **2023**, *10*, 1363-1372.
$\mathrm{CN_{M\text{-}HCl(HT)}}$	0.183	0.1 M KOH	1.23	100 mW cm^{-2}, AM1.5G	*J. Mater. Chem. A* **2024**, *12*, 11502-11510.
CN-MR	0.241	0.1 M KOH	1.23	100 mW cm^{-2}, AM1.5G	*Adv. Funct. Mater.* **2021**, *31*, 2101724.
CN-MSG/M	0.27	0.1 M KOH	1.23	100 mW cm^{-2}, AM1.5G	*Nano Lett.* **2020**, *20*, 4618-4624.
β-FeOOH/CN	0.32	0.1 M NaOH	1.23	AM1.5G	*ACS Appl. Mater. Interfaces* **2023**, *15*, 6726-6734.
$\mathrm{CN_{TM}}$	0.353	0.1 M KOH	1.23	100 mW cm^{-2}, AM1.5G	*Nat. Commun.* **2020**, *11*, 4701.
CN-MR/$\mathrm{NiFeO_xH_y}$	0.472	0.1 M KOH	1.23	100 mW cm^{-2}, AM1.5G	*Adv. Funct. Mater.* **2021**, *31*, 2101724.
PCN	0.65	0.1 M KOH	1.23	100 mW cm^{-2}, AM 1.5G	*Small* **2023**, *19*, 2208049.
K-PHI	0.80	1.0 M NaOH	1.23	100 mW cm^{-2}, AM1.5G	*Chem. Sci.* **2022**, *13*, 7541-7551.
$\mathrm{CN_{TUB}}$	0.87	0.1 M KOH	1.23	100 mW cm^{-2}, AM1.5G	*Small* **2023**, *19*, 2303602.
DCN	0.91	0.1 M $\mathrm{Na_2SO_4}$	1.23	100 mW cm^{-2}, white LED	*Nat. Commun.* **2023**, *14*, 7104.
$\mathrm{Al_2O_3}$|ITO:$^{\mathrm{NCN}}$$\mathrm{CN_x}$	1.40	50 mM 4-MBA in 0.1 M $\mathrm{Na_2SO_4}$	1.23	100 mW cm^{-2}, AM 1.5G	*Angew. Chem. Int. Ed.* **2022**, *61*, e202211587
mpg-$\mathrm{C_3N_4/SnS_2}$/RGO	1.45	0.5 M $\mathrm{Na_2SO_4}$	1.23	40 W white LED, 1 sun	*Int. J. Hydrogen Energy* **2019**, *44*, 11584-11592.

References

(1) Kresse, G.; Hafner, J. *Phys. Rev. B* **1993**, *47*, 558-561.

(2) Kresse, G.; Hafner, J. *Phys. Rev. B* **1994**, *49*, 14251-14269.

(3) Perdew, J. P.; Burke, K.; Ernzerhof, M. *Phys. Rev. Lett.* **1996**, *77*, 3865-3868.

(4) Kresse, G.; Joubert, D. *Phys. Rev. B* **1999**, *59*, 1758-1775.

(5) Blöchl, P. E. *Phys. Rev. B* **1994**, *50*, 17953-17979.

(6) Cao, S.; Yu, J. *J. Phys. Chem. Lett.* **2014**, *5*, 2101-2107.

(7) Cao, S.; Low, J.; Yu, J.; Jaroniec, M. *Adv. Mater.* **2015**, *27*, 2150-2176.

(8) J. Fu; K. Liu; K. Jiang; H. Li; P. An; W. Li; N. Zhang; H. Li; X. Xu; H. Zhou; D. Tang; X. Wang; X. Qiu; Liu, M. *Adv. Sci.* **2019**, *6*, 1900796.

(9) Xia, P.; Cao, S.; Zhu, B.; Liu, M.; Shi, M.; Yu, J.; Zhang, Y. *Angew. Chem. Int. Ed.* **2020**, *59*, 5218-5225.